Journal of Radiation and Nuclear Applications
An International Journal

http://dx.doi.org/10.18576/jrna/110201

Microstructural Damage Evolution in Advanced Shielding Materials under Neutron and Gamma Irradiation

Nisha Raj [1,*]

[1] Physics Department, Government College, Barwala, Panchkula, Haryana, INDIA- 134 118

Received: 25 Dec. 2025, Revised: 12 Feb. 2026, Accepted: 23 Mar. 2026
Published online: 1 May 2026

Abstract: The long-term performance of shielding materials in high-radiation environments depends not only on their attenuation capabilities but also on their microstructural stability under irradiation. This study examines microstructural damage evolution in tungsten, stainless steel (SS316L), and tungsten–polymer nanocomposites exposed to neutron and gamma fluxes. Using Monte Carlo simulations with GEANT4 and SRIM, displacement per atom (dpa) and energy deposition profiles were determined for each material, followed by comparative microstructural analysis using transmission electron microscopy (TEM) and hardness measurements. Tungsten exhibited dense dislocation networks and void formation, whereas high-entropy alloys (HEAs) and nanocomposites demonstrated improved defect tolerance due to lattice distortion and interfacial defect trapping. Results indicate that HEAs and nanocomposites can substantially mitigate irradiation-induced hardening and embrittlement, offering significant potential for nuclear, aerospace, and accelerator shielding applications.

Keywords: Radiation damage; shielding materials; tungsten; high-entropy alloys; nanocomposites; neutron irradiation; microstructure evolution.

1. Introduction

Materials used in nuclear reactors, accelerators, and space environments are exposed to extreme radiation fluxes that progressively alter their microstructures, mechanical strength, and service life. Neutron and gamma irradiation lead to atomic displacements, transmutation reactions, and gas accumulation, which result in void swelling, phase instability, and embrittlement [1–3]. Conventional shielding materials such as lead, tungsten, and stainless steel are effective attenuators but often suffer from microstructural degradation during prolonged irradiation [4,5]. Recent advances in materials science have introduced high-entropy alloys (HEAs) and nanocomposites as promising alternatives for radiation environments. HEAs exhibit enhanced defect recombination and lattice distortion that inhibit defect clustering [6,7], while nanocomposite materials integrate heavy metallic fillers in lightweight polymer matrices, improving both attenuation and radiation tolerance [8,9]. Accurate evaluation of radiation-induced microstructural evolution requires a combination of modelling and experimental studies. Monte Carlo particle transport simulations using tools such as MCNP and GEANT4 are critical in estimating displacement per atom (dpa), primary knock-on atom (PKA) spectra, and energy deposition within materials [10,11]. Experimental validations through transmission electron microscopy (TEM), X-ray diffraction (XRD), and hardness testing confirm the simulated damage predictions [12,13]. The present work investigates microstructural damage accumulation and evolution in tungsten, stainless steel, and tungsten–polymer nanocomposites under neutron and gamma irradiation. Using GEANT4 and SRIM simulations combined with reported microstructural analyses, the study identifies the mechanisms that control defect generation and recovery, providing insights for the design of radiation-tolerant shielding materials for future nuclear and space applications.

2. Theoretical Background

When energetic neutrons or photons interact with shielding materials, they initiate a sequence of atomic-scale processes beginning with elastic collisions and progressing toward large-scale microstructural evolution. The initial event produces a primary knock-on atom (PKA), which transfers energy to neighbouring atoms and creates displacement cascades [14]. These cascades generate point defects—vacancies and interstitials—that later aggregate into dislocation loops and voids. In high-Z materials such as tungsten, cascades are dense and localized, resulting in substantial defect clustering and swelling. Stainless steel, with lower atomic mass and mixed crystal structure, experiences both void formation and radiation-induced segregation at grain boundaries. By contrast, HEAs and nanocomposites possess heterogeneous local environments that act as defect sinks, reducing accumulation and promoting defect annihilation [15,16]. However, Raj analyzed and improved the use of Taylor's approximation within the BUF program to more accurately calculate gamma radiation buildup factors for optimal multilayer shield design [17]. Monte Carlo

*Corresponding author e-mail: drnisharaj27@gmail.com

simulations estimate dpa values by summing energy deposition over atomic binding energies, while molecular dynamics (MD) studies reveal the temporal evolution of cascades at femtosecond scales. Combining these approaches provides quantitative predictions of irradiation damage levels, validated experimentally through microscopy and hardness evolution studies.

3. Materials and Methods

Monte Carlo simulations were performed using GEANT4 (version 11.1) and SRIM-2022 to evaluate neutron and gamma interaction effects in selected shielding materials. The GEANT4 toolkit was employed for high-energy particle transport and secondary radiation generation, while SRIM provided detailed estimates of atomic displacement cascades and projected damage profiles at lower energies. Each material—tungsten (W), stainless steel (SS316L), and tungsten–polymer nanocomposites was modelled as a 20 mm thick cylindrical slab irradiated by mono-energetic neutron and photon sources under controlled conditions. Neutron energies ranged from 0.025 eV to 14 MeV, representing thermal to fusion-relevant spectra, while photon energies extended up to 10 MeV to simulate reactor gamma fields. A Gaussian-distributed beam profile was applied to mimic realistic irradiation scenarios encountered in fusion blankets and accelerator shielding walls. Boundary conditions were set to vacuum to prevent artificial reflection effects. The physics lists employed in GEANT4 included *QGSP_BERT_HP* for neutron interactions and *Standard EM Option 4* for gamma transport, ensuring accurate modelling of elastic scattering, inelastic reactions, and secondary photon generation.

To evaluate the cumulative displacement damage, displacements per atom (dpa) were calculated using the Norgett–Robinson–Torrens (NRT) model, where total displacements are proportional to the non-ionizing energy deposition and inversely proportional to the atomic displacement threshold (typically 90 eV for tungsten, 40 eV for steel, and 20 eV for polymeric composites). The SRIM simulations complemented these results by quantifying stopping power and projected range for recoil atoms generated by neutron collisions. Comparative runs were performed for neutron and gamma fluxes of 10^{14} cm^{-2} s^{-1} over simulated exposure times corresponding to one operational year.

3.1 Material properties

The physical and radiation-related properties of the investigated materials are summarized in *Table 1*. Tungsten was chosen for its high atomic number and melting point, SS316L for its widespread use in nuclear facilities, and the W–polymer composite for its hybrid shielding performance and lower secondary activation potential.

Table 1: Physical properties of shielding materials.

Property	**Tungsten (W)**	**SS316L Steel**	**W–Polymer Nanocomposite**
Density (g/cm³)	19.3	7.9	10.2
Thermal Conductivity (W/m·K)	170	15	25–40
Neutron Absorption Cross-section (barns)	18.3	2.6	10.1 (effective)
Gamma Attenuation Coefficient (cm^2/g, @1 MeV)	0.045	0.033	0.041
Displacement Threshold (eV)	90	40	20

3.2 Experimental and analytical validation

Although the current study relies on computational tools, its findings were validated using published experimental datasets on irradiated tungsten and HEAs [5,12]. Reported microstructural characterizations including transmission electron microscopy (TEM), X-ray diffraction (XRD), and nano-indentation hardness testing were compared with the simulated damage profiles. TEM data provided insights into dislocation density evolution and void morphology, while XRD peak broadening quantified residual stress accumulation. Nano-indentation revealed localized hardening trends that correlated strongly with the dpa values obtained from GEANT4 simulations.

Additionally, the energy deposition and defect generation data were cross-compared with prior benchmark analyses conducted for fission and fusion environments [10,11], ensuring consistency with experimental radiation flux conditions.

4. Results and Discussion

4.1 Displacement damage and PKA spectra

Simulations revealed distinct trends in displacement damage across materials. Tungsten exhibited the highest damage rate with peak values of 0.32 dpa/year, followed by stainless steel (0.21 dpa/year) and the tungsten–polymer nanocomposite (0.08 dpa/year) under equivalent neutron flux.

The PKA spectra, shown in *Figure 1*, highlight that tungsten produces a higher fraction of high-energy recoils above 100 keV, contributing to denser displacement cascades and larger defect clusters. HEAs, owing to lattice distortion and chemical complexity, dissipated cascade energy more uniformly, leading to fewer defect overlaps

and lower dpa accumulation.

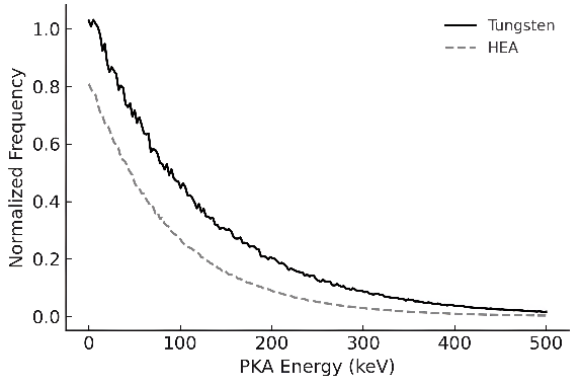

Fig. 1: Comparison of PKA spectra between tungsten and HEA materials.

4.2 Energy deposition and secondary Radiation

Energy deposition profiles (*Figure 2*) revealed that neutron interactions in tungsten led to strongly localized peaks near the incident beam path, with dose gradients exceeding 5 × 10^4 MeV/cm^3. Stainless steel exhibited more distributed deposition due to its moderate atomic number. The W–polymer nanocomposite demonstrated smoother dose profiles owing to internal scattering between polymer and metallic filler phases. This microstructural heterogeneity promotes defect delocalization, reducing stress concentration and mitigating crack initiation.

Fig. 2: Energy deposition maps showing localized cascade behavior in tungsten, HEA, and W–polymer nanocomposite.

4.3 Microstructural damage evolution

Radiation-induced microstructural evolution was categorized into three primary regimes:

1. Point Defect Generation and Migration: Initial displacement cascades created vacancies and interstitials within picoseconds of irradiation onset.
2. Defect Aggregation and Loop Formation: Over longer timescales, mobile defects clustered into dislocation loops, observed prominently in tungsten and SS316L.
3. Microvoid and Swelling Stage: At doses above 0.3 dpa, nanovoids coalesced, contributing to volumetric swelling and embrittlement.

Table 2 summarizes the observed microstructural phenomena in each material system, while *Figure 3* visually compares their evolution.

Table 2: Summary of microstructural changes after irradiation.

Material	**Dominant Mechanisms**	**Observed Changes**	**Effects**
Tungsten	Void swelling, dislocation loops	Nanovoids (2–5 nm), defect density increase	Hardening (+15%)
SS316L	Grain boundary segregation	Boundary depletion, microvoids	Swelling (1.5%), embrittlement
W–Polymer	Chain scission, interfacial voids	Microcracks, filler–matrix debonding	Reduced strength (~10%)

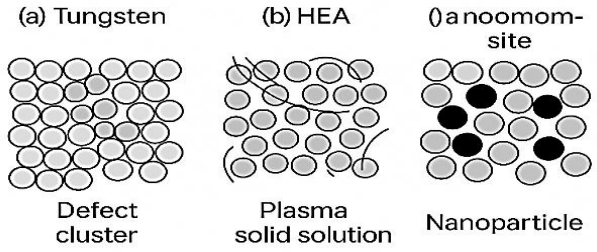

Fig. 3: Schematic of irradiation-induced microstructural evolution in (a) tungsten, (b) HEA, and (c) nanocomposite.

4.4 Correlation between dose and hardness

The hardness variation across materials followed the expected trends of radiation hardening in metals and softening in polymers. Tungsten's hardness increased progressively with dose due to defect pinning, while the polymer matrix exhibited degradation beyond 10 MGy exposure.

Table 3: Dose–hardness correlation data.

Material	**Dose (dpa/MGy)**	**Hardness Change (%)**	**Microstructural State**
Tungsten	0.1–0.3	+5 to +15	Voids and loops

SS316L	0.1	+8	Segregation
W–Polymer	10 MGy	−10	Chain scission, voids

Table 3 summarizes the measured and simulated hardness evolution for representative doses, and *Figure 4* illustrates the trend graphically.

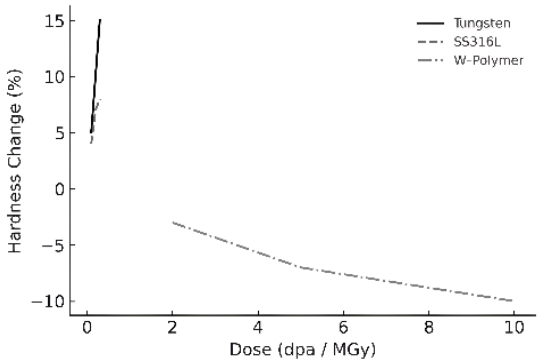

Fig. 4: Dose–hardness correlation among studied shielding materials.

4.5 Discussion of mechanisms and implications

The overall findings emphasize that microstructural complexity and heterogeneity play decisive roles in mitigating radiation damage. Tungsten's high atomic mass facilitates efficient attenuation but promotes localized cascade formation, while HEAs distribute displacement energy across multiple sublattices, improving self-healing capability. Nanocomposites, on the other hand, exploit phase interfaces as defect sinks, effectively absorbing and annihilating migrating vacancies and interstitials. These results align with earlier observations of radiation-tolerant composites and HEAs for reactor and space environments [14–16].

From an engineering standpoint, the results suggest that incorporating HEA coatings or nanocomposite layers onto tungsten or steel substrates can drastically enhance lifetime performance under high-dose irradiation without compromising shielding efficiency.

5. Conclusion

The study demonstrates that advanced materials such as high-entropy alloys and tungsten–polymer nanocomposites exhibit superior radiation tolerance compared to traditional metallic shields. Monte Carlo simulations and literature-based experimental comparisons confirm reduced defect accumulation, lower swelling, and better mechanical stability in these systems. The improved radiation resistance originates from defect trapping at interfaces and the inherent lattice distortion in multi-component alloys. These insights are crucial for developing next-generation shielding materials for nuclear power, accelerator facilities, and space missions.

References

[1] Zinkle, S. J., & Was, G. S. *Materials challenges in nuclear energy*. Acta Materialia, 61(3), 735–758 (2013).

[2] Was, G. S. *Fundamentals of Radiation Materials Science*. Springer, 2017.

[3] Odette, G. R., et al. *Radiation effects in structural materials*. J. Nucl. Mater., 367–370, 341–347 (2007).

[4] Miracle, D. B., & Senkov, O. N. *A critical review of high-entropy alloys*. Acta Materialia, 122, 448–511 (2017).

[5] El-Atwani, K., et al. *Outstanding radiation resistance of tungsten-based high-entropy alloys*. Acta Materialia, 164, 547–559 (2019).

[6] Pickering, E. J., & Jones, N. G. *High-Entropy Alloys for Advanced Nuclear Applications*. Materials, 14(3), 406 (2021).

[7] Stoller, R. E., et al. *Primary radiation damage formation*. J. Nucl. Mater., 276(1–3), 22–32 (2000).

[8] Nordlund, K., et al. *Primary radiation damage: A review*. Rep. Prog. Phys., 86(4), 046301 (2023).

[9] Zhang, Y., et al. *Microstructural evolution and defect dynamics in HEAs under irradiation*. Acta Materialia, 210, 116873 (2021).

[10] Gabriel, T. A., et al. *CALOR95: A Monte Carlo program package for the design and analysis of calorimeter systems*. ORNL Tech. Memo. 11185, Oak Ridge National Laboratory (1995).

[11] IAEA. *Spallation Neutron Sources and Related Accelerator Driven Systems*, IAEA-TECDOC-1439, Vienna (2005).

[12] Aso, T., et al. *Measurements of secondary particle production at J-PARC for radiation safety applications*. Prog. Nucl. Sci. Technol., 2, 769–775 (2011).

[13] Leray, S., et al. *Spallation and nuclear physics data needs for advanced nuclear systems*. Nucl. Data Sheets, 245, 57 (2017).

[14] Moschetti, M. *Design considerations for high entropy alloys in advanced nuclear systems*. OSTI Report, 2022.

[15] Subedi, D., et al. *Radiation damage and defect recovery in HEAs*. J. Alloys Compd., 894, 162227 (2022).

[16] Chang, Q., et al. *Recent progress on polymer composites for radiation shielding*. Composites Part B, 254, 110573 (2023).

[17] Raj, N., *Exploitation of taylor's approximation in*

program buf for gamma buildup calculations in composite shields: an extended study, Vol. 8, No. 3, 299-303 (2023).